ISSN 0021-3640, JETP Letters, 2016, Vol. 103, No. 1, pp. 46–50. © Pleiades Publishing, Inc., 2016.

CONDENSED MATTER

Localized-to-Propagating Surface Plasmon Transitions in Gold Nanoslit Gratings[1]

M. I. Dobynde, M. R. Shcherbakov, T. V. Dolgova, and A. A. Fedyanin

Faculty of Physics, Moscow State University, Moscow, 119991 Russia

e-mail: fedyanin@nanolab.phys.msu.ru

Received November 11, 2015; in final form, December 2, 2015

Plasmon polaritons in thin gold nanoslit gratings with a fixed period and a variable filling factor are studied using microspectroscopy measurements and finite-difference time-domain simulations. The regimes of surface plasmon polaritons, localized plasmons, and the mixed mode are identified.

DOI: 10.1134/S0021364016010057

A surface plasmon polariton is a coherent oscillation of the electron plasma near a metal surface excited by an electromagnetic wave [1, 2]. Two limiting cases of surface plasmons are usually considered. The first is observed in essentially subwavelength metallic nanoparticles; such a localized excitation is termed a localized plasmon polariton (LP) [2–5]. The second represents a travelling wave bound to an infinite metal–dielectric interface and is therefore called a propagating surface plasmon polariton (PSP). The latter is a momentum-carrying wave excited through momentum-matching schemes, e.g., diffraction gratings; plasmonic gratings are widely used as plasmon launchers [6], sensors [7–9], directional emitters [10], polarization converters [11], pulse shapers [12, 13], hyperlens [14], and magnetoplasmonic media [15, 16]. In the gratings, surface plasmons are collective, i.e., neighboring unit cells of the grating are coupled by the plasmonic wave travelling along the metal–dielectric interface. However, if the grating consists of a discontinuous layer of metal—i.e., an array of slits—it is not straightforward to claim the possibility of PSP existence; indeed, increasing the slit width eventually results in isolated nanostripes with LP excitations. Although many studies have been devoted to understanding the coupling between isolated plasmonic nano-objects [17–22] more experimental insights are clearly needed to distinguish between these two phenomena.

In this paper, we explore the transition between the regimes of LPs and PSPs in gold gratings with a fixed period and a variable filling factor. Depending on the slit width, one can identify different plasmon excitation regimes. For slits wider than approximately 0.7 resonant wavelengths, only localized plasmons are present.

As the slit width is reduced, the localized plasmons begin to couple, and weak PSP excitation becomes possible ("plasmon tunneling" regime). The complex spectral behavior of the transmittance in this case reflects the interplay between localized and propagating plasmons. For the narrower slits, the transmittance spectra show features associated with pure PSP excitation.

The samples are five nanogratings with slit widths d of 170, 190, 275, 375, and 500 nm and a period of (750 ± 35) nm. The samples were fabricated by focused ion beam lithography out of a 30-nm-thick gold film deposited on a fused silica substrate. The structured area of each sample is 80×80 μm^2.

Transmittance spectra were measured by using a white-light microspectroscopy setup with a spectral range from 500 to 900 nm, a spectral resolution of 0.8 nm, a focal spot diameter of 25 μm and a numerical aperture of the focusing system of 0.04. The input polarization state was controlled by a Glan–Taylor prism and was either parallel (s-polarization) or perpendicular (p-polarization) to the slits. The nanograting transmittance spectra were normalized to the transmittance spectra of the fused silica substrate.

A difference between the s- and p-polarized light transmittance values was found for all samples. Figure 1 shows the transmittance spectra of s- and p-polarized light for the nanogratings with slit widths of (a) 500 and (b) 170 nm. Transmittance spectra functions measured for the s-polarized light monotonically decay with the increase in wavelength, while the p-polarized light transmittance spectra show features of amplitude and spectral position depending on the slit width d. The key feature of the spectra measured for large slits (500 nm) is the fact that the transmittance of the

[1] The article is published in the original.

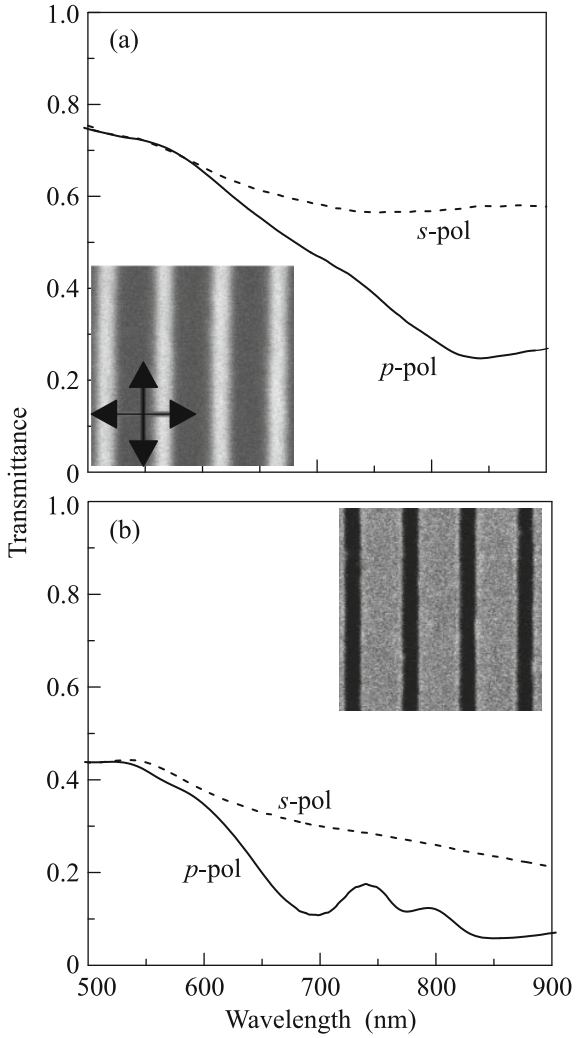

Fig. 1. Normal incidence transmittance spectra for nanogratings with slit widths of (a) 500 and (b) 170 nm. Incident light is linearly polarized (dashed curves) along the stripes or (solid curves) perpendicular to them. Insets show 3 × 3 μm SEM images of the samples; the corresponding light polarization orientation is indicated by arrows.

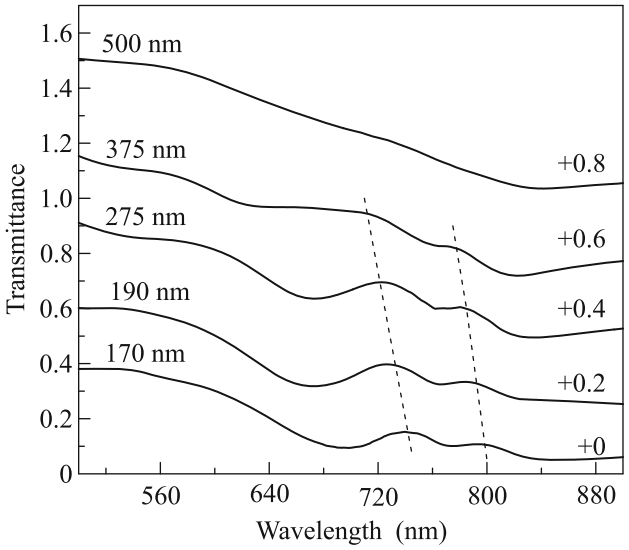

Fig. 2. Transmittance spectra at normal incidence measured in nanogratings with different slit widths for light linearly polarized perpendicular to the nanograting slits. The nanograting period is 750 nm. Values to the left are the slit width values. The spectra are shifted vertically for clarity by the value shown to the right. Dashed lines serve as guides for the eye.

p-polarized light through the samples is lower than that of the *s*-polarized light; moreover, the shape of the *p*-polarized spectra supports the assumption of local plasmons excited in the nanostructure. This assumption is further justified by calculations given below. The transmittance spectrum of the *p*-polarized light through the sample with $d = 170$ nm shows a double peak feature with maxima at 740 and 800 nm. The features are believed to arise because of the PSP excitation at the grating–air interface.

Figure 2 shows the evolution of the *p*-polarized light transmittance spectra with the slit width variation. The slit width increasing leads to the total transmittance increase and the broadening and blue shifting of the transmittance maxima. This indicates the dependence of the PSP dispersion on the slit width [20]. Although the maxima are seen in the spectra of samples with slit widths up to 375 nm, they disappear as the slit width increases to 500 nm.

Figure 3 shows a set of *p*-polarized light transmittance spectra through a sample with a slit width of 170 nm, measured at different angles of incidence θ. The bright stripes in the experimental spectra correspond to PSP resonances. Their positions are calculated from the phase-matching condition

$$\mathbf{k}_{0,x} = \mathbf{k}_{\mathrm{PSP}} + n\mathbf{g}, \quad n = 0, \pm 1, \ldots, \tag{1}$$

and are shown by dashed lines in Fig. 3. Here, $\mathbf{k}_{\mathrm{PSP}}$ is the PSP wave vector, $\mathbf{g}$ is the nanograting reciprocal vector, and $\mathbf{k}_{0,x}$ is the tangential projection of the wave vector of light. The PSP dispersion is assumed to be the same as for a smooth metal film:

$$\mathbf{k}_{\mathrm{PSP}} = \frac{\omega}{c}\sqrt{\frac{\varepsilon_d \varepsilon_m(\omega)}{\varepsilon_d + \varepsilon_m(\omega)}}. \tag{2}$$

Here, ε_d is the permittivity of the dielectric medium (air or silica), $\varepsilon_m(\omega)$ is the permittivity of the metal (gold), ω is the frequency of the incident light, and c is the speed of light in vacuum. The spectral dependence of the gold permittivity is taken from [23] for further calculations.

The nanoscale structuring of the gold film yields the formation of a band gap in the PSP dispersion law that is seen as the transmittance minimum at 760 nm at $\theta = 0°$. Other band gaps contribute to the minima exhibited by the transmittance spectra at the wave-

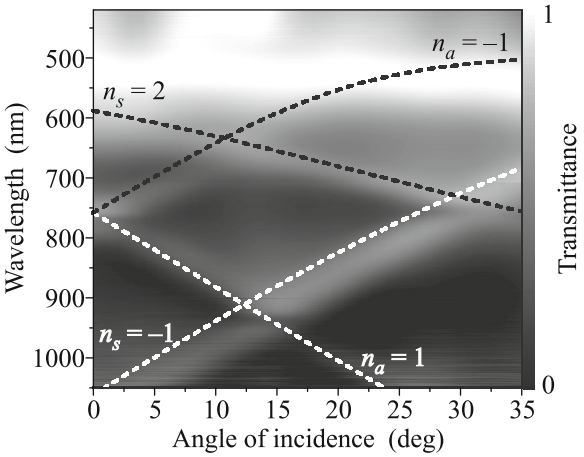

Fig. 3. *p*-polarized light transmittance through the nanograting with a slit width of 170 nm as a function of the wavelength and the angle of incidence. The dashed curves show the dependence of the PSP resonance wavelength calculated from the phase-matching condition; n_a and n_s are the multipliers of the grating reciprocal vector in the phase-matching condition. The subscripts *a* and *s* indicate the gold–air and gold–substrate interfaces, respectively, where the PSP propagates.

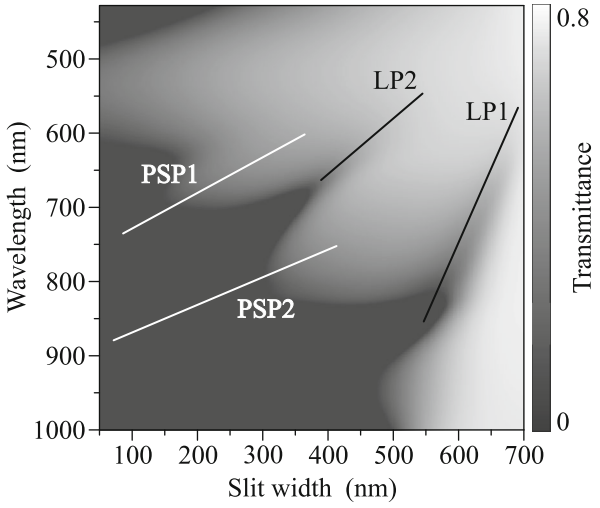

Fig. 4. Simulated transmittance spectra of the nanograting as a function of the slit width *d*. Black lines show the approximate positions of the resonances: PSP1 (2) are the resonances of the surface plasmon polaritons at the gold-air (gold–substrate) interface, and LP1 (2) are the resonances of the localized plasmons.

lengths of 950 and 750 nm, as the angles of incidence are near 15° and 30°, respectively. The transmittance maxima at the band-gap edges are in the opposite directions of the changes in the angle of incidence.

The plasmon oscillation type and its resonance spectral position and width are shown to depend strongly on the slit width. Finite-difference time-domain (FDTD) simulations were applied to show the LP-to-PSP transition in light transmittance through the nanograting with a fixed period of 750 nm and a slit width varying from 50 to 700 nm in the spectral range from 400 to 1000 nm. The series of calculated transmittance spectra is shown in Fig. 4. The transmittance maxima marked as PSP1 and PSP2 are seen in the slit width range from 50 to 400 nm. They are blue-shifted and broadened as the slit width increases. The dips marked as LP1 and LP2 are seen in the slit width range from 300 to 700 nm and become narrower and blue-shifted as the slit width increases.

The type of plasmon excited in the grating can also be retrieved by simulating the electromagnetic energy propagation length spectra. We considered the PSP excitation at an air–gold interface in the Kretschmann prism-coupling configuration shown in Fig. 5a. The old film was thought to be perforated with a periodicity of 750 nm to the right of the excitation region. The electric field intensity distribution $I(x)$ was simulated in the plane parallel to the perforated film at a distance of 300 nm from the gold–air interface and was then fitted to the one-exponential dependence with two adjustable parameters: the amplitude and the PSP propagation length along the nanograting x_{prop}.

The calculated spectral dependences of the propagation length are shown in Fig. 5b for nanogratings with slit widths in the range from 150 to 600 nm and for the unperforated gold film and the gold film edge, i.e., where the slit width is equal to the period. The perforation of the gold film with a periodic array of nanoslits leads to dramatic changes in the propagation length spectra. The spectrum decreases in the long wavelength region, and two maxima appear at the wavelengths of 700 and 800 nm for a slit width of 150 nm. The propagation length value along the perforated film exceeds that for the non-perforated film at a wavelength of approximately 700 nm. Peaks are shifted to 630 and 750 nm as the slit width increases to 300 nm. The propagation length value exceeds one for the non-perforated film at a wavelength of 630 nm (arrow in Fig. 5). The peaks at 640 and 700 nm are observed in the propagation length spectra for the slit widths of 450 and 600 nm.

In an array of periodic metal stripes, *p*-polarized light excites resonant plasma oscillations, producing a complex optical response as the result of simultaneous LP and PSP excitation. LP excitation in plasmonic nanostripes results in a dip in the transmittance spectrum. The metal stripes with slit widths ranging from 250 to 580 nm are wide enough for the excitation of LP resonances. The resonances are broadened as the stripe width increases, eventually overlapping and resulting in transmittance decreases in the red part of the spectrum.

Slit width ranging from 170 to 375 nm are sufficiently small for the PSP to tunnel through the slits, yielding features in the transmittance spectra in the wavelength range from 700 to 800 nm. Light re-emit-

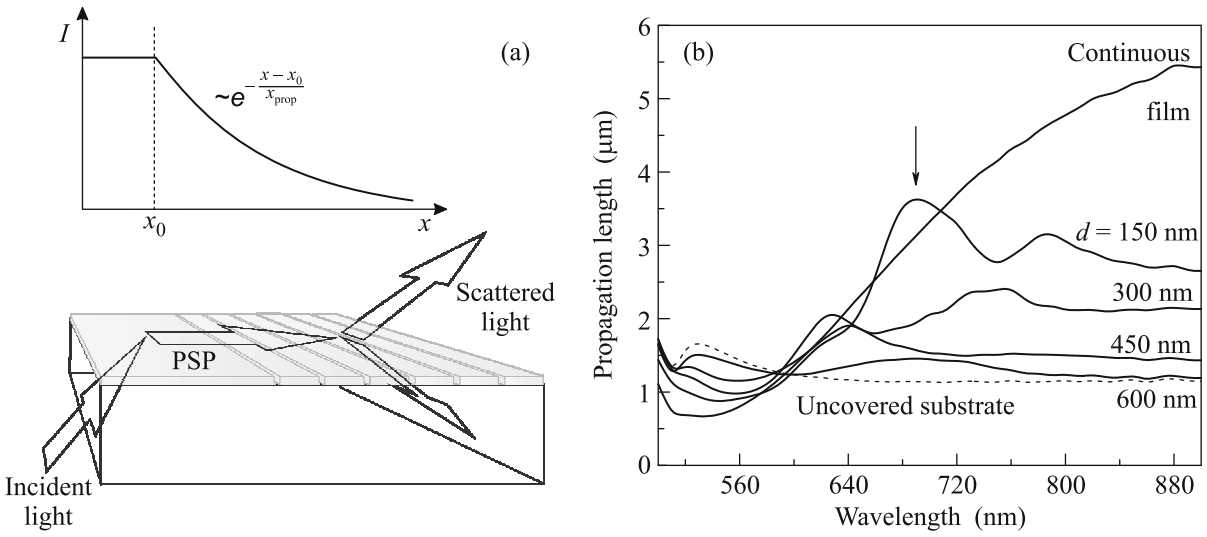

Fig. 5. (a) Schematic representation of the modeled experiment provided to define the PSP propagation length x_{prop}. Propagating surface plasmon polaritons are excited by an incident wave on a smooth gold film using the Kretschmann prism-coupling configuration. The excitation region is to the left of x_0. To the right of x_0, the film is perforated with a period of 750 nm. The PSP amplitude $A(x)$ decays exponentially because of radiative and ohmic losses. (b) The spectral dependence of the PSP propagation length along the nanograting in the x direction. The slit width is varied in the range from 150 to 600 nm with a step of 150 nm; the grating period is set to 750 nm. The black curve shows the propagation length spectral dependence for the smooth film, and the olive curve shows the decay distance of the electromagnetic field at the edge of the gold film.

ted by the PSPs in the forward direction enhances the transmittance, resulting in the maxima observed in the spectral region of PSP excitation. The PSP resonance spectral position is determined by the phase-matching condition (1) that involves the PSP wave vector, nanograting reciprocal vector and tangential component of the light wave vector, which depends on the angle of incidence. The angular dependence of the transmittance maximum position coincides with the calculated one (Fig. 3), confirming their PSP nature.

The transmittance maxima at 740 and 800 nm are yielded by PSP modes excited at the edges of the plasmonic band gap that are formed because of the periodicity of the gold nanograting. The spatial distribution of the electromagnetic field energy in these modes is different, and the concentration of energy is located either above the slits or above the gold stripes. Thus, the experimental nanoslit samples can be treated as one-dimensional plasmonic crystals showing plasmonic band gaps analogous to photonic crystals with band gaps for photons [21].

The peaks in Fig. 4 marked as PSP1 and PSP2 appear because of PSP excitation at the gold–air and gold–substrate interfaces, respectively. They are shifted by 150 nm to the shorter wavelength region as the slit width increases from 50 to 400 nm. Unlike the experimentally observed transmittance peak, the PSP1 peak is not split, and consequently, there is no plasmonic band gap. This mismatch is a result of the difference between the designs of the simulated structure and the real one. Both resonance peaks are broadened as the slit width increases, indicating that the PSP lifetime and propagation length decrease as the slit width increases.

Figure 4 also provides information about the region of the large slit width values that were not experimentally tested. The transmittance spectrum of the nanograting with a slit width of 700 nm shows a 100-nm-wide dip at 600 nm resulting from the LP excitation in each stripe. This spectrum shifts to longer wavelengths and broadens as the stripes become wider, which is typical for such resonances. The dip in Fig. 4 at 600 nm marked LP2 is caused by the second-order LP resonance, which appears as the slit width reaches 500 nm, and exhibits behavior similar to that of LP1. The spectral features for wavelengths smaller than 550 nm are determined by the interband transitions of gold and are typical of bulk gold.

The interpretation of the simulated spectra in the regions of very narrow or very wide slits is rather simple. Narrow slits support PSP oscillations, while wide slits support LP ones. This is not the case for intermediate slit widths between 250 and 450 nm, which correspond to filling factors from 0.7 to 0.4. The transmittance spectrum can be explained by a set of LP resonances and a set of PSP ones. The maxima of the PSP resonance could be formed between dips of the LP one and, in the same fashion, the dips of LP could arise between the maxima of PSP.

Changing the slit width exerts different influences on the propagation length in different spectral regions. The presence of slits and the increase in their width produce a monotonic transmittance decrease in the long wavelength region because of the spatial confine-

ment of electron movement at lengths smaller than the half of the PSP wavelength. This spatial limitation makes it impossible to create the necessary charge density in the grating plane, and thus, the PSP cannot efficiently propagate along the nanograting surface. This leads to a propagation length reduction to 50% at a wavelength of 900 nm in comparison with that along the non-perforated film. Another situation occurs in the shorter wavelength region, where the spatial localization of the electron movement is comparable to the wavelength. The propagation length spectrum of the sample with a slit width of 150 nm has maxima at 690 and 790 nm. The propagation length value at 690 nm exceeds that for the non-perforated film by a factor of 1.2. The propagation length dependence is more complex for the larger slit widths, as seen by comparing the blue curve, corresponding to a slit width of 300 nm, with the red one. The absolute value positions of both the peaks and the dips depend on the slit width. The propagation length spectrum for the grating with a slit width of 300 nm shows a maximum at 620 nm, which also exceeds the propagation length value along the non-perforated gold film. Considering the middle spectral region and increasing slit width, maxima can be seen at 630 and 700 nm as the slit widths reach 450 and 600 nm, respectively, which are related to the mixed excitation of LP and PSP. As a result, the field energy is redistributed over the nanograting, and the propagation length spectrum exhibits a complex dependence on the slit width. For slit widths larger than 450 nm, the propagation length is almost spectrum insensitive (violet and gold curves in Fig. 5b). The propagation length dependence on the slit width is weak at wavelengths longer than 700 nm and does not benefit from propagation length improvement. Therefore, 450 nm is determined to be a critical slit width value: above this value, PSP cannot effectively propagate in nanoslit gratings with a period of 750 nm.

In conclusion, three regimes of plasmon excitation in thin gold nanoslit gratings are described experimentally and numerically. The plasmon excitation regimes are distinguished according to the different effects of localized and propagating surface plasmons on the transmittance spectra of nanogratings with a period of 750 nm. Varying the slit width from 170 to 500 nm allows switching between the regimes. Pure localized plasmons are found in the stripes for slits wider than 450 nm, yielding decreased transmission. A complex spectral behavior of the transmittance is shown in the slit width region from 250 to 450 nm, reflecting the interference interplay between localized and propagating plasmons. Features associated with propagating surface plasmons are observed in the transmittance spectra for slits narrower than 250 nm; a blue shift in the propagating plasmon resonances as the slit width increases is observed both experimentally and numerically. Additional simulations of the near-field intensity distribution over the nanogratings clarify these values, revealing the decay lengths for different nanogratings.

The work was supported by the Ministry of Education and Science of the Russian Federation (project no. ID RFMEFI61314X0029).

REFERENCES

1. H. Raether, *Surface Plasmons* (Springer, Berlin, 1988).
2. M. Kauranen and A. V. Zayats, Nature Photon. **6**, 737 (2012).
3. F. J. Garcia de Abajo, Rev. Mod. Phys. **79**, 1267 (2007).
4. J. N. Anker, W. P. Hall, O. Lyandres, N. C. Shah, J. Zhao, and R. P. Van Duyne, Nature Mater. **7**, 442 (2008).
5. B. B. Tsema, Y. B. Tsema, M. R. Shcherbakov, Y. H. Lin, D. R. Liu, V. V. Klimov, A. A. Fedyanin, and D. P. Tsai, Opt. Express **20**, 10538 (2012).
6. E. Devaux, T. W. Ebbesen, J. Weeber, and A. Dereux, Appl. Phys. Lett. **83**, 4936 (2003).
7. J. Homola, I. Koudela, and S. S. Yee, Actuat. B **54**, 16 (1999).
8. C. Caucheteur, Y. Shevchenko, L.-Y. Shao, M. Wuilpart, and J. Albert, Opt. Express **19**, 1656 (2011).
9. W.-K. Kuo and C.-H. Chang, Opt. Express **18**, 19656 (2010).
10. M. Toma, K. Toma, P. Adam, J. Homola, W. Knoll, and J. Dostlek, Opt. Express **20**, 14042 (2012).
11. M. R. Shcherbakov, M. I. Dobynde, T. V. Dolgova, D. P. Tsai, and A. A. Fedyanin, Phys. Rev. B **82**, 193402 (2010).
12. M. R. Shcherbakov, P. P. Vabishchevich, V. V. Komarova, T. V. Dolgova, V. I. Panov, V. V. Moshchalkov, and A. A. Fedyanin, Phys. Rev. Lett. **108**, 253903 (2012).
13. P. P. Vabishchevich, M. R. Shcherbakov, V. O. Bessonov, T. V. Dolgova, and A. A. Fedyanin, JETP Lett. **101**, 787 (2015).
14. J. Sun, M. I. Shalaev, and N. M. Litchinitser, Nature Commun. **6**, 7201 (2015).
15. A. A. Grunin, A. G. Zhdanov, A. A. Ezhov, E. A. Ganshina, and A. A. Fedyanin, Appl. Phys. Lett. **97**, 261908 (2010).
16. P. P. Vabishchevich, A. Yu. Frolov, M. R. Shcherbakov, A. A. Grunin, T. V. Dolgova, and A. A. Fedyanin, J. Appl. Phys. **113**, 17A947 (2013).
17. G. Schider, J. R. Krenn, W. Gotschy, B. Lamprecht, H. Ditlbacher, A. Leitner, and F. R. Aussenegg, J. Appl. Phys. **90**, 3825 (2001).
18. E. M. Hicks, S. Zou, G. C. Schatz, K. G. Spears, R. P. van Duyne, L. Gunnarsson, T. Rindzevicius, B. Kasemo, and M. Kll, Nano Lett. **5**, 1065 (2005).
19. G. Vecchi, V. Giannini, and J. Gomez Rivas, Phys. Rev. Lett. **102**, 146807 (2009).
20. I. I. Smolyaninov, A. V. Zayats, A. Gungor, and C. C. Davis, Phys. Rev. Lett. **88**, 1874021 (2002).
21. W. L. Barnes, T. W. Preist, S. C. Kitson, and J. R. Sambles, Phys. Rev. B **54**, 6227 (1996).
22. M. R. Shcherbakov, A. T. Le, N. Dubrovina, A. Lupu, and A. A. Fedyanin, Opt. Lett. **40**, 1571 (2015).
23. P. B. Johnson and R. W. Christy, Phys. Rev. B **6**, 4370 (1972).